JGR Atmospheres

RESEARCH ARTICLE
10.1029/2018JD029751

A Case Study of the Transport/Transformation of Air Pollutants Over the Yellow Sea During the MAPS 2015 Campaign

Hyo-Jung Lee[1], Hyun-Young Jo[1], Shin-Young Park[1], Yu-Jin Jo[1], Wonbae Jeon[1], Joon-Young Ahn[2], and Cheol-Hee Kim[1]

[1]Department of Atmospheric Sciences, Pusan National University, Busan, South Korea, [2]Climate and Air Quality Research Department, National Institute of Environmental Research, Incheon, South Korea

Key Points:
- The existence of the elevated mixed layer was observed and simulated during the MAPS-Seoul 2015 campaign
- The pollutants within the elevated mixed layer pass above the marine boundary layer and travel longer over northeast Asia
- Aerosol concentrations have increased along the elevated mixed layer as the gas phase precursors move across the Yellow Sea

Supporting Information:
- Supporting Information S1

Correspondence to:
C.-H. Kim,
chkim2@pusan.ac.kr

Citation:
Lee, H.-J., Jo, H.-Y., Park, S.-Y., Jo, Y.-J., Jeon, W., Ahn, J.-Y., & Kim, C.-H. (2019). A case study of the transport/transformation of air pollutants over the Yellow Sea during the MAPS 2015 campaign. *Journal of Geophysical Research: Atmospheres*, *124*, 6532–6553. https://doi.org/10.1029/2018JD029751

Received 4 OCT 2018
Accepted 29 APR 2019
Accepted article online 17 MAY 2019
Published online 27 JUN 2019

Author Contributions:
Conceptualization: Hyo-Jung Lee
Data curation: Joon-Young Ahn
Formal analysis: Hyo-Jung Lee, Hyun-Young Jo, Shin-Young Park, Yu-Jin Jo
Investigation: Wonbae Jeon
Methodology: Cheol-Hee Kim
Supervision: Cheol-Hee Kim
Validation: Hyun-Young Jo, Shin-Young Park
Writing - original draft: Hyo-Jung Lee
Writing – review & editing: Cheol-Hee Kim

©2019. American Geophysical Union. All Rights Reserved.

Abstract As a case study, the fate of pollutants subjected to long-range transport over northeast Asia was investigated. These pollutants originated as emitted particulate pollutants from Chinese source area, moved across the Yellow Sea (YS), and entered the Korean Peninsula (KP) during the Megacity Air Pollution Studies Seoul (MAPS-Seoul) 2015 aircraft field campaign. The MAPS-Seoul campaign, designed as a precampaign of the Korea-United States Air Quality (KORUS-AQ) campaign, was performed to diagnose the air quality around the KP and YS. Of particular interest during the campaign period was the existence of the elevated mixed layer (EML), the lofted layer of highly concentrated fine aerosols, observed in the marine atmosphere in and around the western coast of the KP. The pollutants within EML identified with the bulk Richardson number of 1.2–6.1, transported longer toward the downwind area than within marine boundary layer. As a result, pollutants emitted from Chinese source areas can cross the YS due to the EML and influence the surface air quality on downstream areas, where the inland boundary layer is sufficiently developed. We also analyzed the vertical distribution of the simulated sulfur dioxide (SO_2) and sulfate (SO_4^{2-}) in the EML over China-YS-KP belt area and found that the concentration of SO_4^{-2} increases through a hygroscopic conversion process as the gas phase precursors move across the YS in an environment full of water vapor. Therefore, the EML makes the transport of the Chinese plume possible, as it passes over the marine boundary layer, entering downwind area over northeast Asia.

1. Introduction

Rapid industrial development in East Asia, specifically in China, has resulted in unprecedented growth in anthropogenic emissions, inducing air quality issues over neighboring areas. In East Asia, the fate of long-range transported pollutants emitted from China is one of the most important issues in terms of both scientific interest and political concern. Many studies have revealed numerically and observationally that transboundary transport processes of the Chinese outflow are one of the most important factors in the presence of air pollutants over its neighboring countries. For example, ozone and ozone precursors emitted from China are found to be transported to the western United States via long-range transport (LRT) processes over the North Pacific Ocean by taking advantage of the processes that induce the chemical transformation of ozone precursors to ozone (Liang et al., 2004; Lin et al., 2012; Liu et al., 2003; Zhang et al., 2008).

In addition to ozone, the impact of the LRT of various species such as carbon monoxide, sulfur dioxide, anthropogenic aerosols, and natural dust from China on air quality levels over neighboring countries has been widely examined (Carmichael et al., 2002; Li et al., 2010; Li et al., 2012; Lin et al., 2005; Park et al., 2005; Uno et al., 2009). They showed that the LRT of pollutants plays an important and growing role in determining the atmospheric composition and air quality at populated locations remote from the sources (Holzer et al., 2005). In particular, analysis of intensive observations during the U.S.-China joint research project EAST-AIRE (East Asian Study of Tropospheric Aerosols: An International Regional Experiment) 2005 field campaign has demonstrated that SO_2 columns and aerosol optical depth (AOD) of Chinese pollutant plumes increased during the LRT phenomena (Li et al., 2007).

The horizontal pathway and impacts of long-range transported air pollutants have been fully examined though various previous studies (Chun et al., 2001; Kwon et al., 2002; Park et al., 2005; Kim et al., 2008; Choi et al., 2013; Jeong et al., 2013; Sun et al., 2013; Kim et al., 2016; Kim et al., 2017). Recent studies

have focused on the secondary formation of aerosol components over Korean Peninsula and near Yellow Sea, with emphasis on horizontal transport pathways of pollutants over northeast Asia (Kim et al., 2018). On the other hand, vertical mixing structures of air pollutants and their transport downwind from major industrial/urban areas over northeast Asia, such as Shanghai and Shandong in China, were not well studied, but only a few studies have associated with vertical structures of transported air pollutants (Dickerson et al., 2007; Li et al., 2010; Miao et al., 2018). At present, the lack of in situ vertical measurements may be the biggest hurdle at present, and therefore, the chemical transformation of Chinese air pollutants across the ocean remains a crucial part of the phenomenal analysis in northeast Asia.

It has been widely known that the local planetary boundary layer (PBL) is one of the major uncertainty factors in predicting local air quality, particularly in stagnant meteorological conditions, whereas special attention has not been paid to the LRT process. However, our air quality analysis showed that uncertainties remain as to whether the local PBL in the source region can have an important bearing on a receptor's air quality, even for LRT cases. Therefore, attention should be given to reduce uncertainties about how the PBL in the source regions can affect the air quality level in the receptor regions, given the favorable meteorological conditions of LRT situated over northeast Asia.

From May to June 2015, an intensive field campaign—MAPS-Seoul (Megacity Air Pollution Studies-Seoul) 2015 research project, a pre-campaign of the Korea-United States Air Quality (KORUS-AQ) campaign—has been conducted by the Korean Environment Administration. The campaign was designed to characterize the chemical evolution of oxidants and aerosol in and out of the Korean Peninsula, and also to diagnose the three-dimensional transport pathways through the source and receptor regions. Several scientific flights were conducted around the western coastal areas in the Korean Peninsula (KP) and above the Yellow Sea (YS), located between eastern China and the KP (Figure 1). The related comprehensive modeling studies have also been conducted to diagnose the air quality of Seoul (the capital of South Korea), relating to the chemical evolution, transboundary contribution, and improvement of emission inventories.

In this study, one fate of LRT of Chinese air pollutants under a specific meteorological condition is presented as a case study, suggesting the importance of the PBL in both source and receptor regions. In addition, the existence of the elevated mixed layer (EML) in the marine atmosphere is characterized during the MAPS-Seoul 2015 campaign period, and the chemical transformation processes within the EML is revealed. Its importance in the chemical predictions for shorter timescales, such as 2- or 3-day forecasts of $PM_{2.5}$ concentrations over the KP, is also discussed.

2. Methods

2.1. In Situ Measurements

The MAPS-Seoul aircraft measurements were performed from 18 May to 13 June in 2015 over the west coastal area of South Korea, which includes the Seoul and its surrounding cities, and coastal areas over the YS, which is located between China and the KP. The HanSeo King-Air aircraft (Textron Aviation Inc.), cooperated by the University of HanSeo and the Korean Environmental Administration, was used. The aircraft mission was conducted to study the particulate matter over Seoul and its west coastal regions by measuring mass concentrations of particulate matter and its chemical components such as inorganic species (including sulfate, nitrate, and ammonium) and organic aerosol (OA). There have been no aircraft measurements for gas species such as SO_2, NO_x, and O_3 concentrations during the MAPS-Seoul campaign.

On board were high-resolution time-of-flight aerosol mass spectrometer (HR-ToF-AMS) and an ultra-high sensitivity aerosol spectrometer for detecting organics, sulfate, nitrates, and ammonium (Lee et al., 2015). Hereafter, HR-ToF-AMS was refer to as AMS in this study. The HanSeo King-Air conducted seven science flights over the area covering from the YS to the eastern coastal city (Kim et al., 2018). All seven flights were equipped with the AMS onboard.

The operation of the AMS is based on ambient air pulled through a cyclone at a flow rate of 3 L/min to remove particles with aerodynamic diameters larger than 2.5 μm in front of the AMS. Ambient air enters the AMS through a pressure drop critical orifice 110 μm in diameter with an average inlet flow rate of 0.105 L/min. An aerodynamic lens focuses ambient particles of ~35 nm to ~1 μm into a narrow beam to create the particle beam, which then flows into the particle time-of-flight region. Nonrefractory particles,

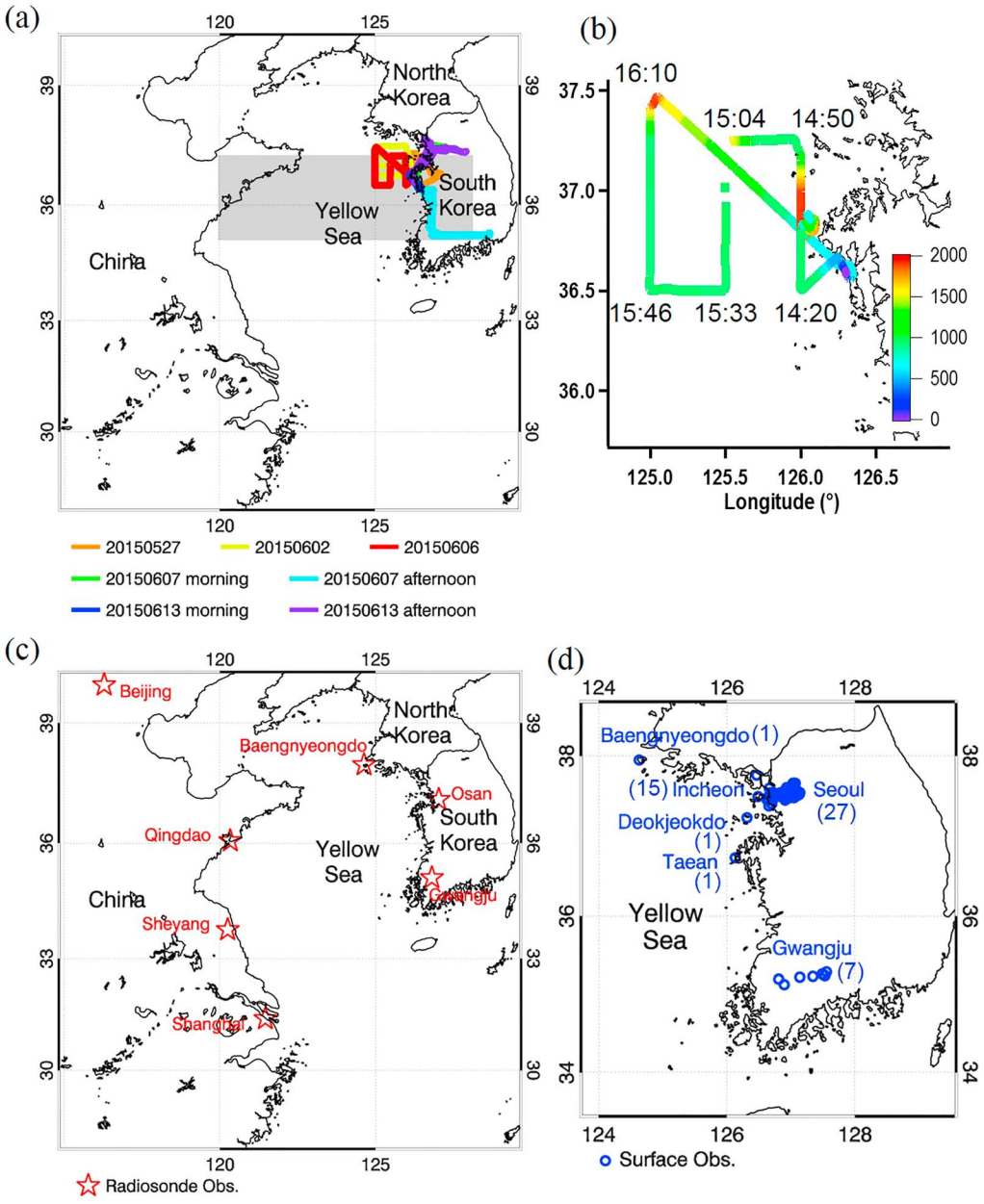


Figure 1. (a) HanSeo King Air flight pathways during Megacity Air Pollution Studies-Seoul 2015 campaign and (b) flight path on 6 June 2015. Also shown are the geographic locations of the (c) radiosonde and (d) surface observation sites in China and Korea, used in this study. The gray shaded area in (a) is for latitude-averaged curtain plots in Figures 9 and 10, and numbers in parentheses in (d) indicate numbers of surface observation sites.

with the aerodynamic diameter of $d < 1$ μm, are vaporized on impact with a resistively heated surface at ~600 °C and ionized by electron ionization at 70 eV. All these make it difficult to measure the $PM_{2.5}$ with the diameter of more than 1 μm through an aircraft inlet. The detailed operation is described elsewhere (i.e., Canagaratna et al., 2007; DeCarlo et al., 2006; Drewnick et al., 2005; Jayne et al., 2000; Jimenez, 2003; Lee et al., 2015).

During the MAPS-Seoul 2015 campaign period, the HR-ToF-AMS was operated under V-mode, and an MS mode of 20-s time resolution was used to determine the compositions of nonrefractory particles including the concentrations of organic aerosol (OA), nitrate, sulfate, ammonium, and chloride. The HR-ToF-AMS was calibrated for ionization efficiency by using 350-nm ammonium nitrate particles at a number density

of ~300 cm^{-3}. The values of the relative ionization efficiency for other aerosol types including organic aerosol, sulfate, nitrate, ammonium, and chloride were derived from default values (Lee et al., 2015).

Figure 1a presents the seven pathways of aircraft flights conducted during the MAPS-Seoul 2015 campaign period. We focus on the flight observations over the marine area, the YS, to identify the transport and chemical evolution of LRT of Chinese plumes, as indicated in Figure 1a. Aircraft flight path with flight time for 6 June 2015, employed as a LRT case in the current study, is presented in Figure 1b. The King Air aircraft measured mixing ratios of air pollutants up to 2 km above ground on 6 June 2015, starting from Taean to the northern part of the YS, the northern ocean area located between Shandong peninsula and Seoul (Figure 1b). Over the ocean area of the YS, we examined the detailed vertical characteristics of in situ measurements together with WRF-Chem (Weather Research and Forecasting model coupled to Chemistry) model results to see the transport/transformation of air pollutants during the LRT processes.

For the evaluation of the WRF-Chem model performance, additional in situ meteorological data were employed, including rawinsonde observations of water vapor mixing ratios in Beijing (116.28°E, 39.93°N), Qingdao (120.33°E, 36.06°N), Sheyang (120.25°E, 33.76°N), Baengnyeongdo (124.63°E, 37.97°N), Osan (127.03°E, 37.10°N), and Gwangju (126.81°E, 35.11°N), as indicated in Figure 1c. The rawinsonde data have been downloaded from the Upper-Air Data Center, which operates in the Department of Atmospheric Science at the University of Wyoming (http://weather.uwyo.edu/upperair/sounding.html). The provided rawinsonde data were grouped into three parts: mandatory levels, significant temperatures, and significant winds. The data used here are in the mandatory levels category, and they consist of temperature, humidity, winds, and heights at specified pressure levels (1,000, 925, 850, 700, 500, 400, 300, 200, and 100 hPa; Lee et al., 2014). Rawinsonde data for Gwangju and Osan stations located both in the western coastal area in South Korea has been compiled with six-hourly observations (00 UTC, 06 UTC, 12 UTC, and 18 UTC), while other Chinese stations were measured twice a day (00 UTC and 12 UTC).

In situ surface measurements of both O_3 and PM_{10} concentrations were also employed for model evaluations. The measurements were collected at three urban stations and three rural sites in South Korea. Detailed information about the in situ observation sites are presented in Figure 1d.

2.2. Satellite Observations

In order to evaluate the simulated spatial distribution, we used satellite observations from Ozone Monitoring Instrument (OMI) aboard Aura, which was launched in 14 July 2004 as a polar-orbiting satellite. Aura has a local equator-crossing time of 13:45 in the ascending node (Lamsal et al., 2010; Levelt et al., 2006). The OMI instrument has a 2,600-km wide swath and a spatial footprint of 13×24 km^2 at its nadir. In our study, the OMI tropospheric NO_2 data set retrieved by The Royal Netherlands Meteorological Institute (KNMI) was utilized to offer a basis for a qualitative, and not quantitative, comparison against the modeled spatial distribution of Chinese plumes during the study period when highly polluted plumes were located over the YS. The tropospheric NO_2 columns provided by KNMI were acquired from the website (http://www.temis.nl/airpollution/no2.html).

2.3. Model Description

The model used here is the WRF-Chem (version 3.8.1), three-dimensional chemical transport model, which was developed at the National Center for Atmospheric Research in collaboration with several research institutes. It is a comprehensive chemistry model coupled with the WRF community model, a nonhydrostatic mesoscale numerical weather prediction model. WRF is a meteorological model with operational flexibility and computational efficiency, and it offers advances in physics, numerical methods, and data assimilation contributed by the research community (Skamarock et al., 2008).

The WRF-Chem model is an "online" system in the sense that all processes resulting from the gas phase and aerosol species interact with the meteorological dynamics (Grell et al., 2005). In our WRF-Chem modeling study, the horizontal domain of 173×128 grid cells has a grid spacing of 27 km, and the vertical grid is composed of 15 full sigma levels, which are 1.000, 0.996, 0.990, 0.980, 0.964, 0.922, 0.894, 0.860, 0.817, 0.766, 0.644, 0.507, 0.380, 0.228, 0.121, and 0.000, respectively. Meteorological initial and boundary conditions were taken from 6-hourly $1° \times 1°$ National Centers for Environmental Prediction/Final Analysis data (National Centers for Environmental Prediction, 2000). Due to coarse resolution ($1° \times 1°$) of initial

meteorological data and coarse designations of sea-land surface over the complex coastal areas, relatively poorer model performance has been expected against that of fine resolution model. Other physical options for WRF meteorological model were Mellor-Yamada-Janjic (MYJ) boundary layer physics (Janjic, 2002), the NOAH land surface model (Chen & Dudhia, 2001), a Rapid Radiative Transfer Model (RRTM) longwave and Goddard shortwave radiation schemes (Iacono et al., 2008), and the Grell-Freitas ensemble cumulus parameterization with radiative feedback and shallow convection (Grell & Freitas, 2014).

The WRF-Chem model has various chemical mechanisms available. We used a chemical scheme named Regional Atmospheric Chemistry (RACM)-Earth System Research Laboratory (ESRL; Kim et al., 2009) for gas phase chemistry. RACM-ESRL was an updated version of the Regional Acid Deposition Model (RADM), developed based on the chemical mechanisms of RADM2 and RADM-Mainz Isoprene Mechanism (MIM). The RADM2 photochemical mechanism was originally developed by Stockwell et al. (1997), and used most intensively in previous WRF-Chem studies, and the RACM-MIM mechanism was updated with rate coefficients following the Jet Propulsion Laboratory 2006 report (Sander et al., 2006) and multiple references (Orlando et al., 2002; Tyndall et al., 2001). For our aerosol chemistry, the Modal Aerosol Dynamics model for Europe/Secondary Organic Aerosol Model (MADE/SORGAM) mechanism (Ackermann et al., 1998; Schell et al., 2001) was applied.

The chemical boundary conditions for the main trace gases and particulate matter concentrations were provided by simulations by the Model for Ozone and Related Chemical Tracers (MOZART) (Emmons et al., 2010). In the chemical initial condition process, this study employed the model containing reinitialized National Centers for Environmental Prediction meteorological fields for each day of a 5-day run, recognized as sufficient for the initial conditions of chemical variables to reach equilibrium.

All of the above mechanisms were compiled using the Kinetic Preprocessor method coupled with the WRF-Chem model (see automatic coding of chemistry solvers in WRF-Chem). A paper describing this method was presented by Salzmann and Lawrence, at the 7th WRF/16th MM5 Users' Workshop, National Center for Atmospheric Research, Boulder, Colorado, 2006, available at http://www.mmm.ucar.edu/wrf/users/workshops/WS2006/abstracts/Session06/6_4_Salzmann.pdf.

As an emission input data set, the used anthropogenic emission inventory for East Asia, Comprehensive Regional Emissions inventory for Atmospheric Transport Experiment (CREATE) was compiled by two research groups: Kon-Kuk University and the National Institute of Environmental Research, South Korea, which was also used for both MAPS-Seoul and KORUS-AQ campaigns (Woo et al., 2014). The CREATE emission inventory includes the Multi-resolution Emission Inventory of China (MEIC) (http://www.meicmodel.org/), Clean Air Policy Support System (CAPSS) (http://airemiss.nier.go.kr), and Regional Emission Inventory in Asia version 2 (http://www.jamstec.go.jp/frsgc/research/d4/emission.htm). The detailed information on CREATE emission was well documented in Woo et al. (2014). The employed biogenic emissions were derived by using the Model of Emissions of Gases and Aerosols from Nature (MEGAN) version 2 emission module (Guenther et al., 2006). Sea salt emission and biomass burning emission (based on FINN module) were both considered in WRF-Chem simulation, whereas dust emissions were not included here, as there were no dust reports during our case study period.

3. Results

3.1. Case Selection—Long-Range Transport Process Case

In this study, 6 June in 2015 was chosen as a long-range transport (LRT) case. The issue of classification: long-range transport versus stagnant case for seven flight days during the MAPS-Seoul 2015 campaign was discussed in detail by Kim et al. (2018). For the classification, they employed several synoptic variables suggested by Jo and Kim (2013). Figure 2 depicts weather charts at two levels: 850 hPa and surface pressure over the period from 5 to 6 June in 2015. A low-pressure system at 850 hPa emanating from northern mainland China stagnated over the area between the northeastern part of China and Mongolia, and another low pressure system moved from the southeastern part of South Korea to southwestern mainland Japan. Accordingly, westerlies prevailed all day over the YS, due to the synoptic wind direction blowing in parallel with isobar lines on the 850-hPa level. On surface weather charts (Figure 2a), on 5 and 6 June 2015, a low-pressure zone formed over the area from the Beijing-Shandong-Shanghai region, extending to the western

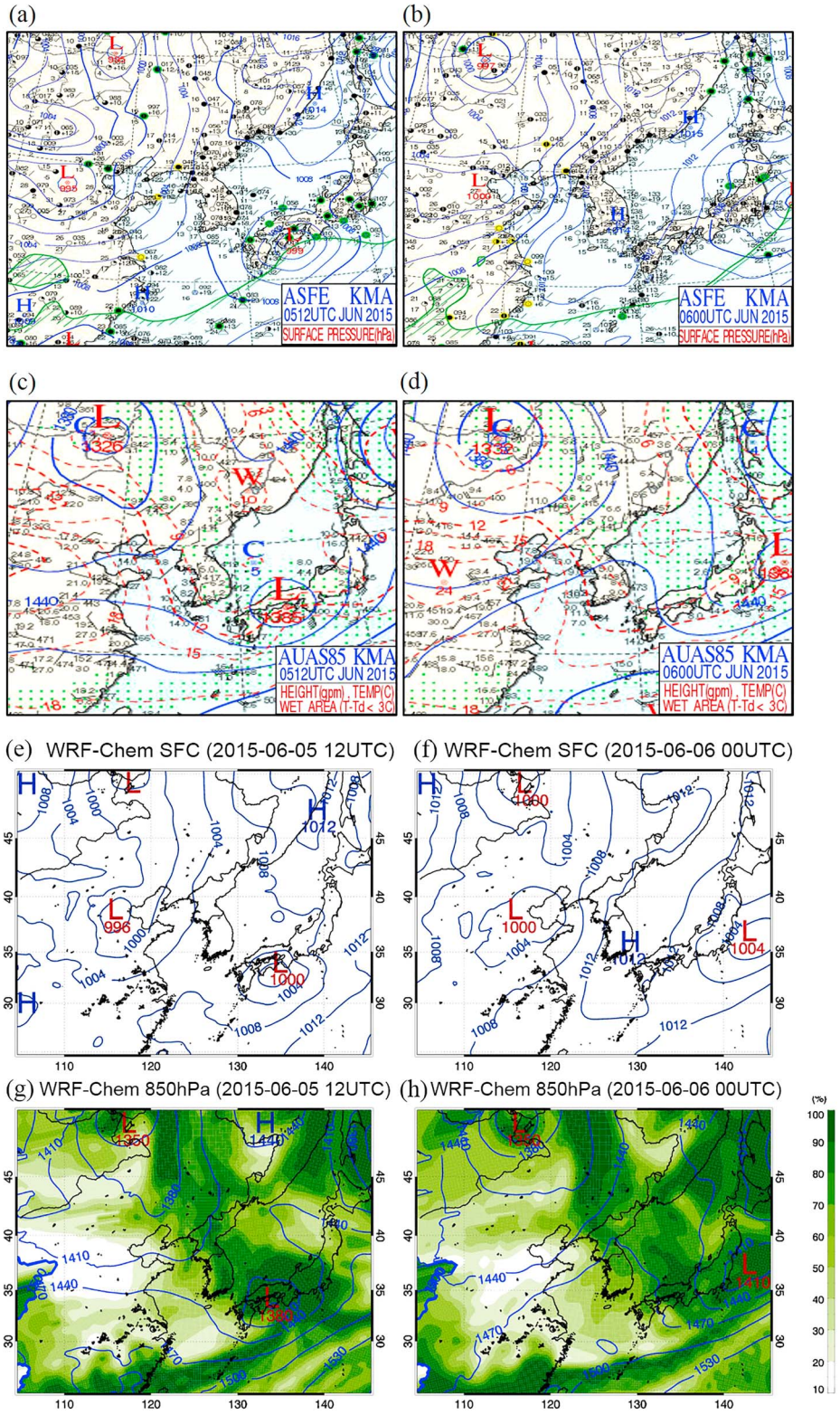


Figure 2. Weather maps (Korean Meteorological Administration) for long-range transport (LRT) case (6 June 2015). Surface pressures charts are shown for (a) 12 UTC 5 on June 2015 and (b) 00 UTC on 6 June 2015, and 850-hPa charts are for (c) 12 UTC on June 5, and (d) 00 UTC on 6 June 2015. Here (e)–(h) are the same as (a)–(d) but for Weather Research and Forecasting model coupled to Chemistry (WRF-Chem) model results. Highlighted areas in green are indicating $T - T_d$ < 3 °C in (a)–(d), and contour lines with green shadings are for depicting relative humidity in (g)–(h).

part of South Korea with southeasterlies (or southerlies) over the area of the YS. We identified this synoptic pressure as a well-placed prepositioning of the LRT mechanism where Chinese outflow could influence downwind areas from the surface to upper atmosphere.

In this study, 2 June in 2015 was also chosen as a non-LRT case, and its synoptic charts at two levels: 850 hPa and surface pressure were shown in Figure 3. The synoptic characteristics for this non-LRT case was also found in Kim et al. (2018). Figures 2, 3 illustrated the comparisons between weather charts and modeled pressure fields (surface and 850-hPa level) for two cases: 6 June (LRT case) and 2 June (non-LRT case). We identified this synoptic pressure of 6 June in 2015 as a well-placed prepositioning of the LRT mechanism where Chinese outflow could influence downwind areas from the surface to 850-hPa atmosphere (Figure 2). On the other hand, 2 June in 2015 was recognized to be non-LRT case with relatively lower surface wind speed over the Korean Peninsula under the presence of both broad and weak low pressure located over North Korea and high pressure over northwest China (Figure 3). Overall, the modeled high/low pressure pattern simulated by the WRF meteorological model also shows good agreement with the analysis of the two weather charts, along with model performance without special biases for both cases (see Figures 2, 3).

To evaluate the simulated meteorological variables in more detail, simulated vertical profiles of wind speed/directions were compared against rawinsonde observations over three regions: one island (Baengnyoengdo) and two inland regions (Osan and Gwangju), during 5–6 June 2015 (Figure S1 in the supportng information). Figure S1 also showed the good agreements between observations and simulations, with no significant biases except for some surface wind speed, overall showing low root-mean-square error, and index of agreement of more than 0.7 in most regions, as indicated in Table S1. The only poorer performance with the correlation coefficient (R) of 0.46 for temperature in Baengnyoengdo would be partly caused by the coarse resolution of initial meteorological data (section 2.3) with the poor designation of sea-land surface over the complex coastal areas, while observations are obtained at fixed point. Thus, incorporation of more detailed surface designation might yield better wind fields with the use of finer horizontal resolution.

During the total MAPS-2015 campaign period, observed mean levels of SO_2 are less than ~10 ppb for both Seoul and Baengnyoengdo in 2015. The observed daily mean PM_{10} levels during the MAPS-Seoul campaign period ranged between 27.0 and 53.7 $\mu g/m^3$ over Seoul Metropolitan Area, which agreed well with a seasonal average of 43.7 $\mu g/m^3$ in spring (March to May). In this study, 6 June in 2015 (LRT case) yielded that daily averages of PM_{10} were 30.4 (maximum 49.6) $\mu g/m^3$ and 28.3 (maximum 49.2) $\mu g/m^3$ in Seoul and Gwangju, while Baengnyoengdo showed the average of 26.9 (maximum 60.0) $\mu g/m^3$, respectively. It indicated no appreciable differences among three regions, while island region, Baengnyoengdo showed relatively higher variation compared with other two urban inland regions, Seoul and Gwangju. On 2 June 2015 (non-LRT case), averages of PM_{10} observed 35.7, 47.2, and 27.8 $\mu g/m^3$ in Seoul, Gwangju, and Baengnyoengdo, respectively, with the maximum of 47–58 $\mu g/m^3$. It shows bigger differences among three regions in non-LRT case. Other detailed characteristics including seasonality of PM_{10} in and around Seoul Metropolitan Area were found (Kim et al., 2017).

Model performances of $PM_{2.5}$ were evaluated against aircraft measurements for 6 June in 2015 (Figure S2). In Figure S2, observed mass concentration levels are in the range of 5–50 $\mu g/m^3$ with a mean value of 19.8 $\mu g/m^3$, whereas model showed higher (55 ± 10 $\mu g/m^3$) than observations by a factor of approximately 2.5. However, sulfate, which is larger portion of $PM_{2.5}$ chemical components, compares well between simulations and observations, and nitrate and ammonium have higher values in simulations, but no appreciable differences were found (Figure S2).

WRF-Chem results showed relatively higher estimation for total mass concentrations than individual sulfate, nitrate, and ammonium species. This is partly because model essentially calculate all of chemical components including sea salt, elementary carbon, and other chemical components.

Figure 4 shows the horizontal distributions of three tropospheric NO_2 columns: OMI satellite observations, WRF-Chem simulations with and without applying OMI averaging kernel to WRF-Chem model simulations for both two cases: LRT case (6 June 2015) and non-LRT case (2 June 2015). In Figures 4b and 4d, WRF-Chem output was interpolated and smoothed in time and space to locations of satellite retrievals and convolved with the OMI averaging kernels used in the satellite retrievals (Kumar et al., 2012). Scatterplot comparisons of NO_2 columns between OMI-retrieved versus WRF-Chem simulations by applying OMI

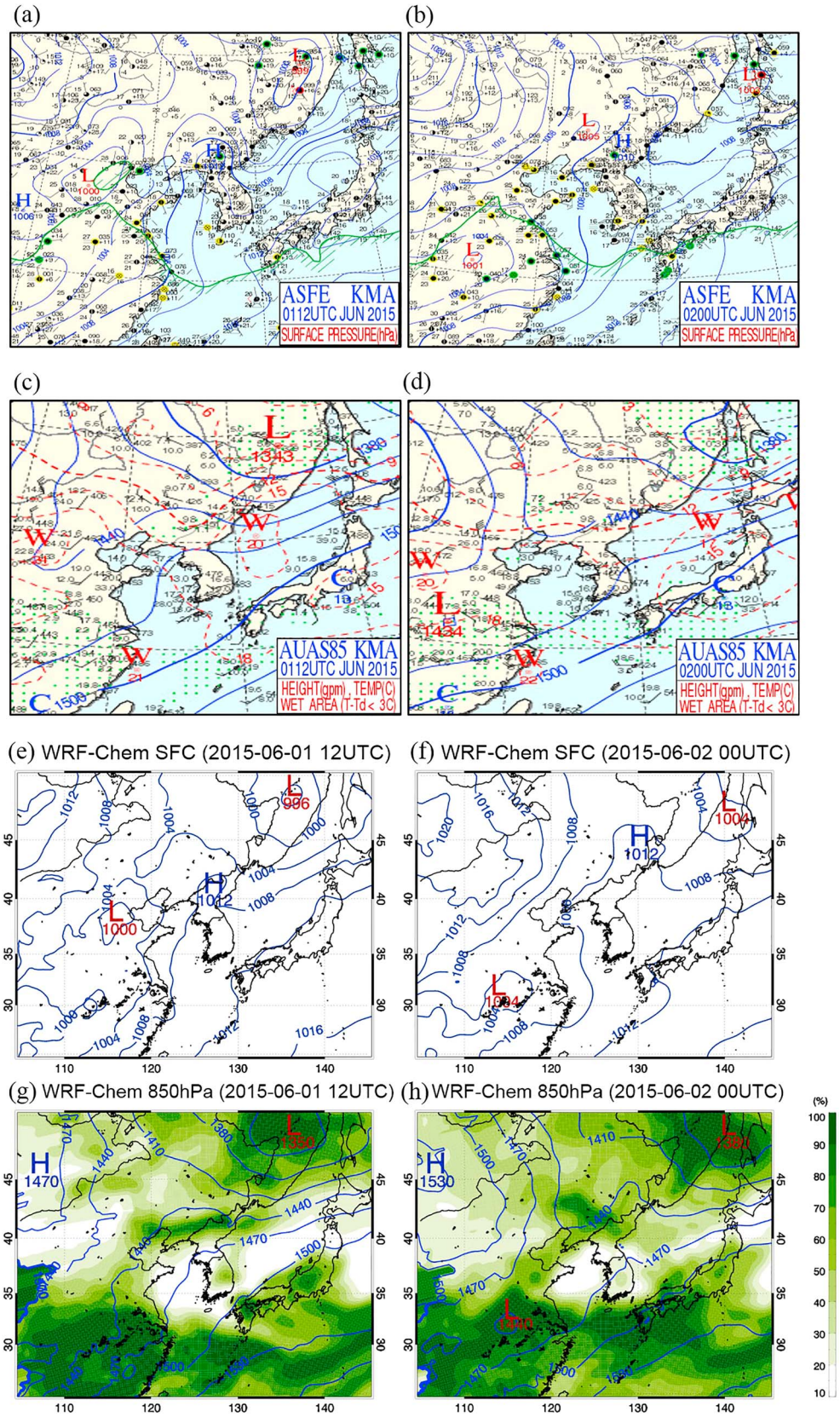


Figure 3. The same as Figure 2 but for non-LRT case (2 June 2015).

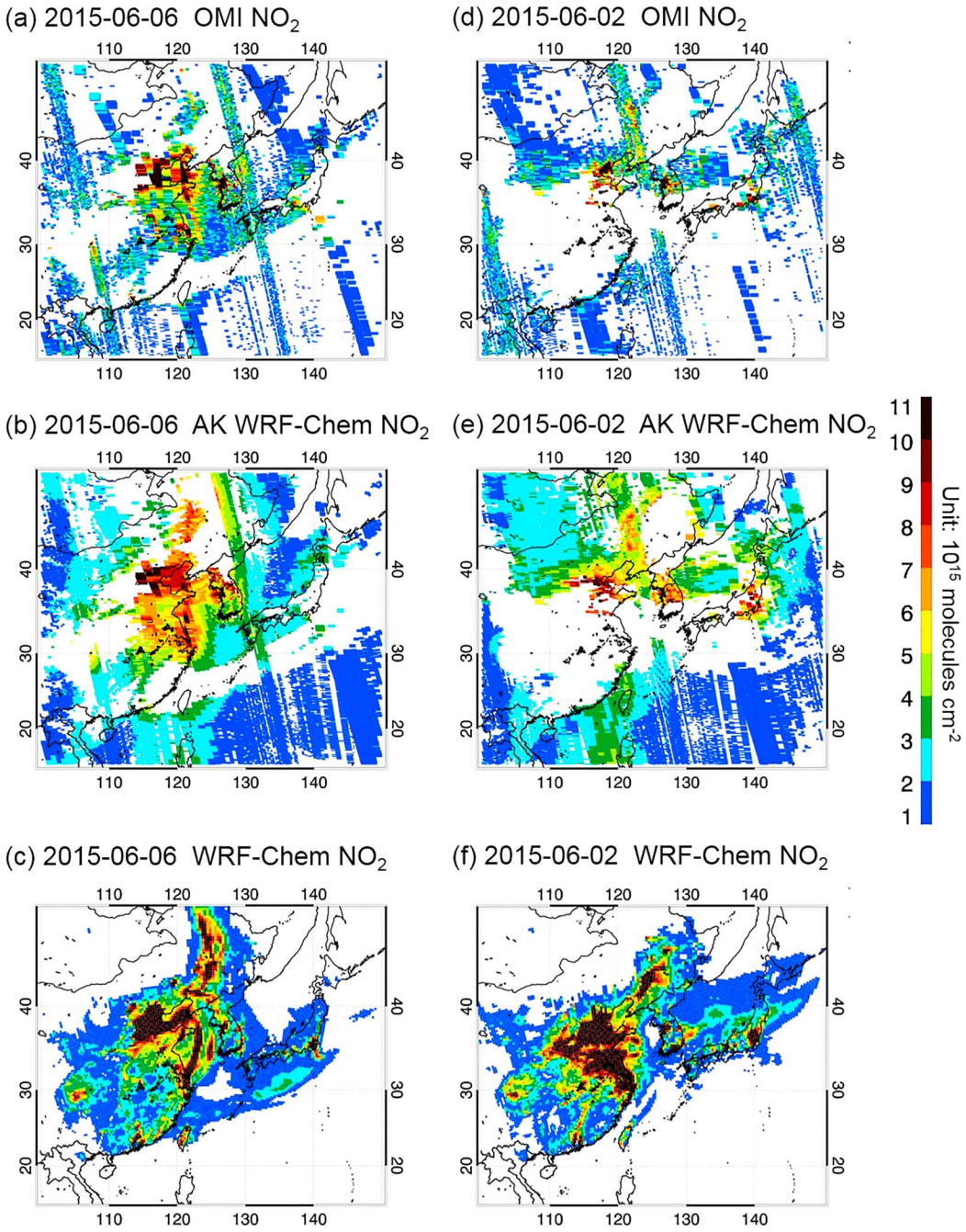


Figure 4. Tropospheric NO_2 columns on 6 June 2015 (a–c) and 2 June 2015 (d–f): OMI-Retrieved (a, d); WRF-Chem simulations by applying OMI averaging kernel to model profile (b, e); and WRF-Chem simulations without applying averaging kernel (c, f).

averaging kernel for both two cases were found in Figure S3. In Figure 4 and Figure S3, although some underestimations of WRF-Chem simulations were found in some places, it is overall indicating that a significant LRT process occurred on 6 June 2015, and WRF-Chem model also captured the transported horizontal structures of Chinese plumes over the YS more clearly than on 2 June 2015.

3.2. Horizontal Transport Pathway as Seen From Modeling and Observation

Figure 5 describes a time series of hourly measurements and simulated PM_{10} and O_3 concentrations at the surface in Seoul together with several rural and coastal sites near the YS, on 6 June 2015. We employed PM_{10}

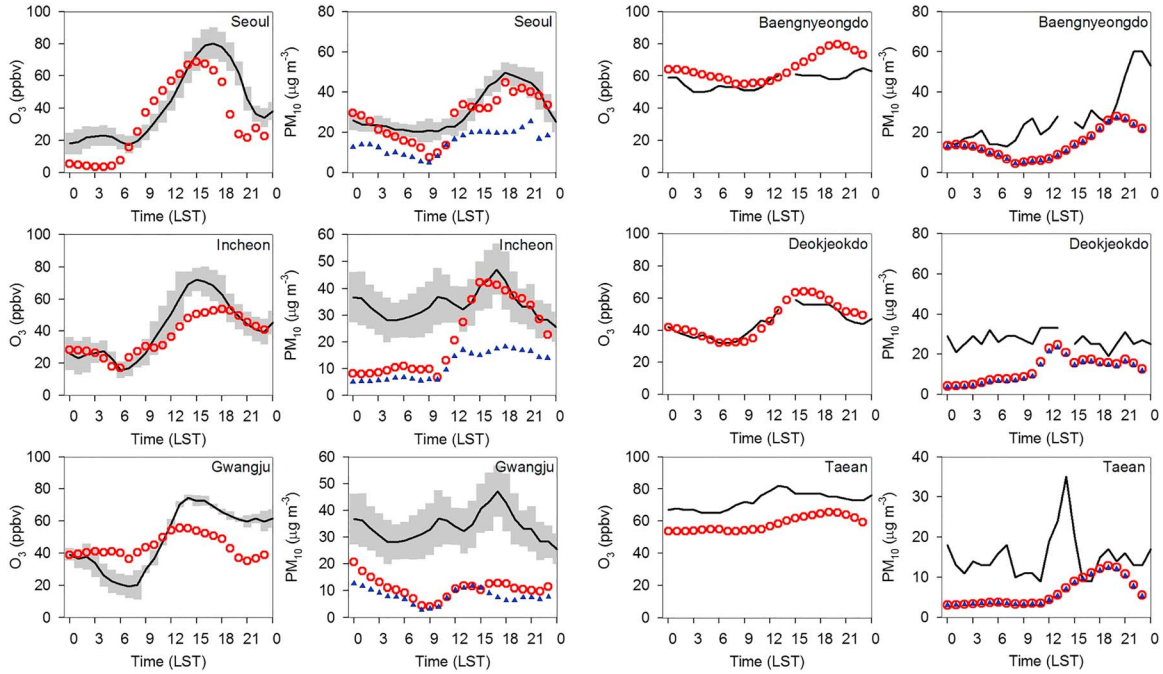


Figure 5. Observed and simulated hourly O_3 (left panels), and PM_{10} and $PM_{2.5}$ concentrations (right panels) on 6 June 2015, over three western coastal cities (Seoul, Incheon, and Gwangju) and three rural areas (Baengnyeongdo, Deokjeokdo, and Taean) in South Korea. The open red circles and closed blue triangles indicate Weather Research and Forecasting model coupled to Chemistry simulated PM_{10} and $PM_{2.5}$, respectively, and the black lines and gray shadings represent the mean values and standard deviations of the observation data set.

here because of nonavailability of $PM_{2.5}$ observations for two sites: Taean and Deokjeokdo. The results show that the model reproduces the observed diurnal variations and concentration levels of PM_{10} and O_3 in Seoul and Baengnyeongdo (Figure 1d), showing agreement with the range of maxima. The simulated maxima times, recorded at 18:00–21:00 LST, were also in agreement with observations of PM_{10}. Here LST is UTC +09:00 and +08:00 in Korea and China, respectively. However, higher discrepancies between the observed and simulated PM_{10} concentrations were found during the morning over the southern coastal sites: Baengnyeongdo, Taean, and Deokjeokdo, as indicated in Figure 1d. However, in all regions, both modeled and observed PM_{10} show enhanced surface concentrations from 11:00 LST. These might not be caused by regional and/or local pollutant emissions. However, because local emissions are small for most coastal sites such as Taean and Deokjeokdo, these enhancements are believed to be influenced by LRT phenomena. Over several western coastal areas where there were no local emissions, this simultaneous increase since around 11:00 LST in both observed and simulated $PM_{2.5}$ concentrations implies mesoscale phenomena (i.e., LRT) of air mass such as a Chinese emission-ridden air mass and its transport toward the KP.

The spatial distributions of modeled $PM_{2.5}$ concentrations at both surface and 850-hPa level on 5–6 June in 2015 are shown in Figure 6a (left panel) and Figure 6b (right panel), respectively. Differences in transport pathways of air pollutants between surface and upper levels were clearly found over the area of the YS. In particular, at the 850-hPa level, the prevailing westerlies over inland areas (110–120°E, 30–40°N) in China led to the accumulation of air pollutants in the atmosphere along the shoreline during 06:00–18:00 LST on 5 June. On the surface, however, from 00:00 LST on 6 June, the Chinese plumes did not move across the YS toward the KP from 00:00 LST on 6 June due to a dominant southerly flow over the subarea zone of Shandong-YS belt area. Hence, the northern area of the YS was weakly influenced by LRT pollutants, with no (or only a slight) increase in $PM_{2.5}$ concentrations in the lower atmosphere (Figure 6). The results are consistent with no (or small) increases in $PM_{2.5}$ concentrations, reflected in surface observations in Baengnyeongdo and Seoul during the morning on 6 June as indicated in Figure 5. On the other hand, surface $PM_{2.5}$ concentrations in Incheon, Gwangju, Deokjeokdo, and Taean did not increase on that day. To investigate the discrepancies shown in the model against observations during 0:00–10:00 LST on –6 June, further analysis of the local $PM_{2.5}$ emissions at each site would be required.

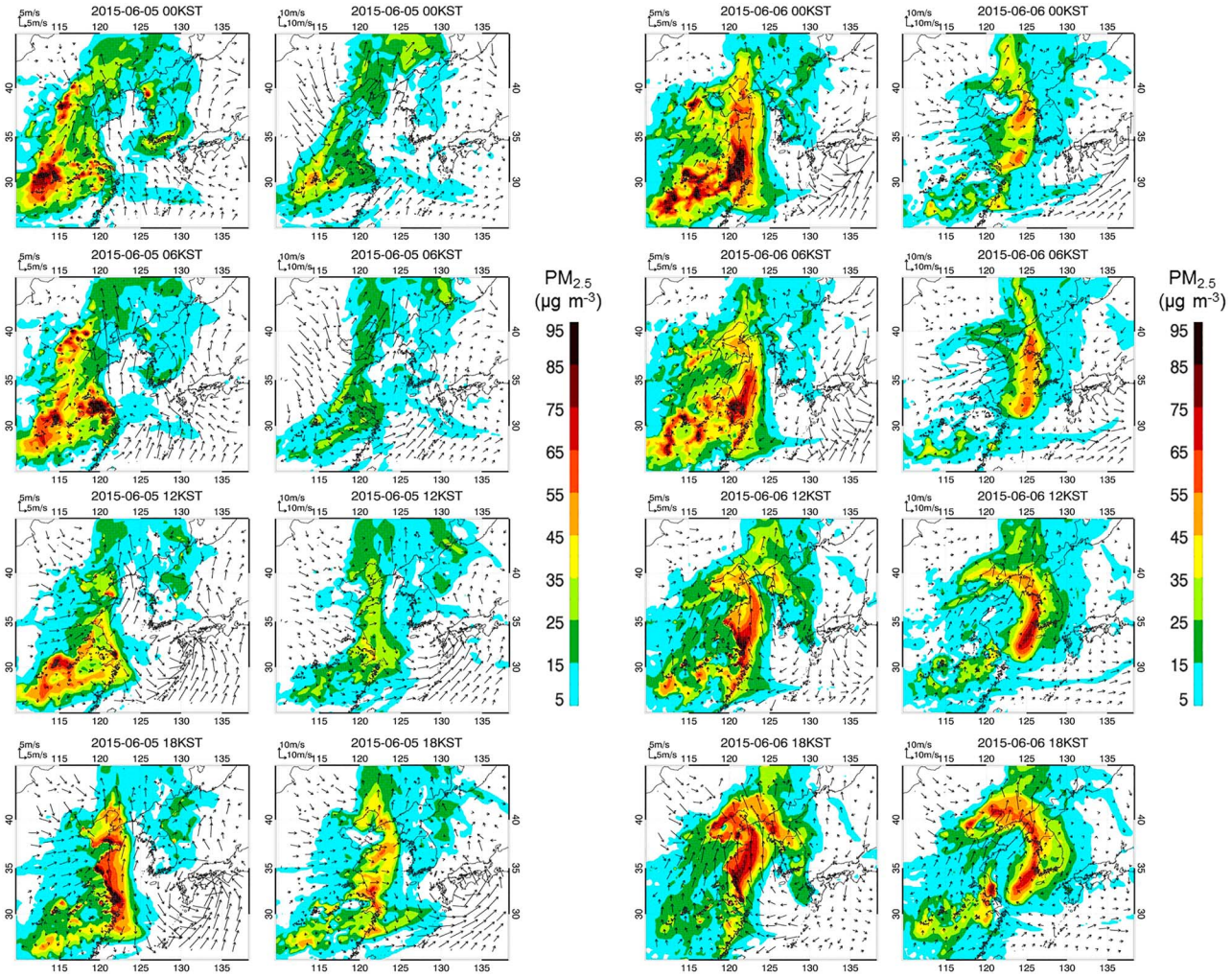


Figure 6. Horizontal distributions of modeled $PM_{2.5}$ at surface (left panels) and at 850 hPa (right panels) during 5–6 June 2015.

However, in the upper atmosphere (i.e., at 850 hPa height) on 6 June in 2015, the Chinese plume affected the air quality over downwind areas much more considerably, as described in the spatial distributions of $PM_{2.5}$ at around 850-hPa height (Figure 6). The Chinese plume began to move from central China at 00:00 LST and then stretched to the eastern coastlines of China at 12:00 LST on 5 June 2015. As a result, enhanced $PM_{2.5}$ concentrations were found at 850-hPa height over the Shanghai-Shandong area with belt shape concentration features extending south and north during the early nighttime on 5 June. This pattern was formed due to the merging of the transported plume that was lifted to upper altitudes over central China. On 6 June 2017, the model result shows Chinese plumes sweeping down eastward over the western regions of the KP, in accordance with strong and pervasive westerlies over the YS. This implies that upstream plumes at the higher altitude can pass through the marine atmosphere without removal process such as dry deposition and dissolving process on the ocean surface. They can accordingly cause the prevalence of the surface $PM_{2.5}$ concentrations through the entrainment at the top of the PBL and the vertical mixing process within the PBL in the downstream atmosphere.

3.3. EML Above Marine Boundary Layer

As shown in the horizontal pathway of LRT plumes on 5–6 June, most pollutants flowed into the KP through the upper level of the YS. As it was expected that the marine boundary layer (MBL) plays a large role in the pollutant transport process, we analyzed the properties of the vertical structure in two separated areas: exit (upwind) and entrance (downwind) areas. The exit area is referred to as a subregion covering the northeast

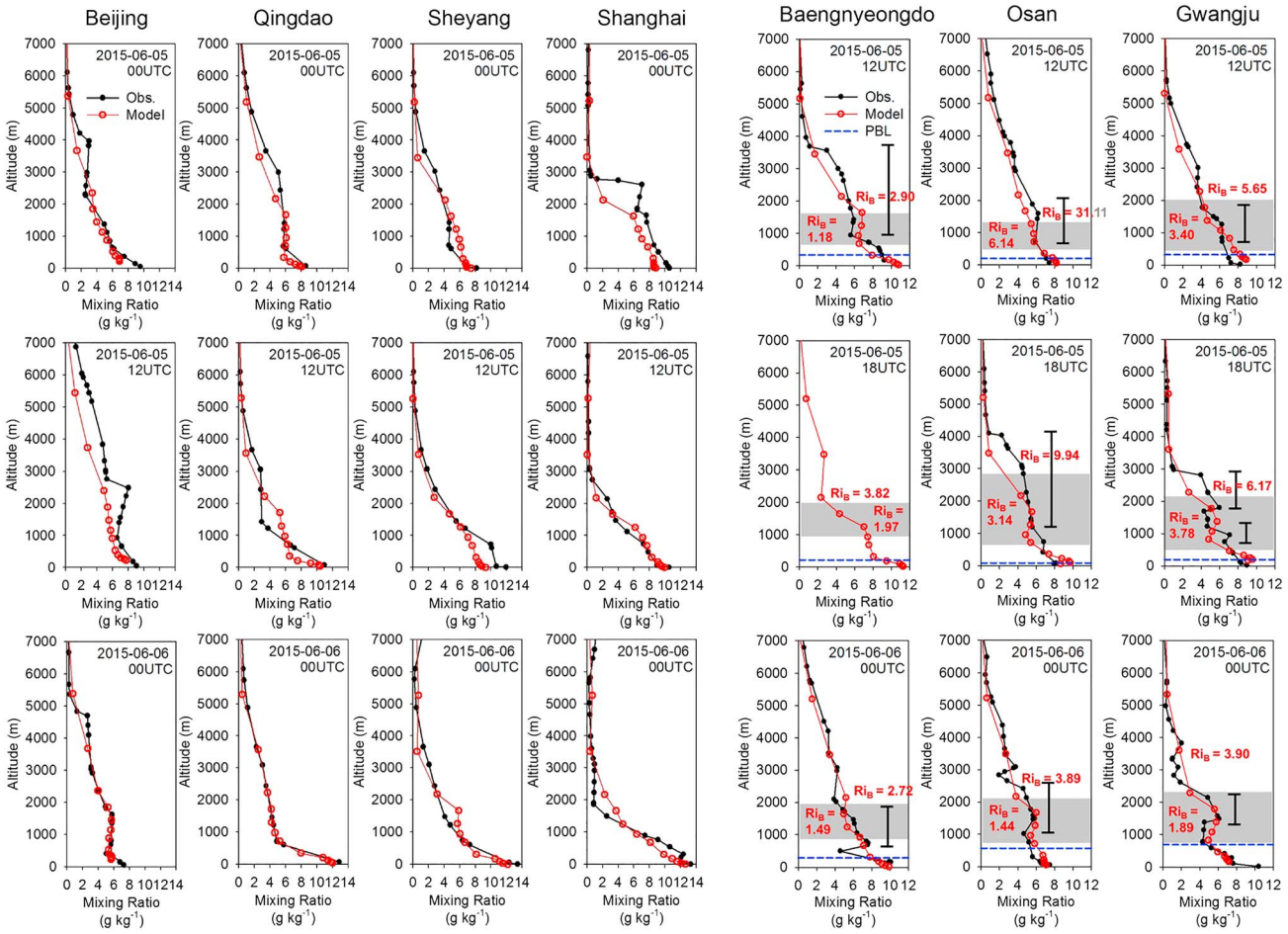


Figure 7. The vertical profiles of the Weather Research and Forecasting model coupled to Chemistry simulated water vapor (red lines with open circles) and Rawinsonde observations (black lines with close circles) above upwind areas (Beijing, Qingdao, Sheyang, and Shanghai) located in the central/eastern coastal region in China, and downwind areas (Baengnyeongdo, Osan, and Gwangju) in the Korean peninsula. Ranges of elevated mixed layers: vertical bars (black solid lines) depict estimation from Rawinsonde observations, and gray shadings are from model simulations. Bulk Richardson number, Ri_B, is also denoted here.

Chinese mainland to the YS, and the entrance area covers the northeastern YS, partly including the interior of the KP's west coast.

The detailed vertical transport processes are examined by performing a comparative analysis of two data sets: the amount of water vapor measured by rawinsonde and the simulated water vapor vertical profile. As a model validation step, we first evaluated the accuracy of the WRF-Chem simulations of the atmospheric PBL height and lofted (elevated) mixed layer over the exit and entrance areas: China's east coast areas and west coast region of Korea.

Figure 7a shows the vertical distributions of the water vapor mixing ratios in Beijing, Qingdao, Sheyang, and Shanghai, which are all located on the windward side (see Figure 1). These are good locations in mainland China to delineate as exit areas, where pollutants would be raised to higher altitudes due to the developed PBL in China before flowing into the marine atmosphere of the YS. In Figure 7, relatively higher mixing ratios were observed in Beijing (exit area) at 00 UTC on 5 June and were found up to the layer near 3,000–4,000 m. We interpreted this layer formed as a result of relevant synoptic low-pressure activities rather than turbulent mixing process: simulated turbulence intensities were found to be extremely high with a bulk Richardson number (Ri_B) of greater than 10.0 and, in some cases, greater than 100. Here bulk Richardson number, $Ri_B = (\frac{g}{\theta_v})(\theta_{v2} - \theta_{v1})\,(z_2 - z_1)/[(u_2 - u_1)^2 + (v_2 - v_1)^2]$, where g is gravity, θ_v is virtual potential temperature, u and v are components of wind speed, and subscripts, 1 and 2, mean lower and upper altitudes, respectively.

However, at 12 UTC on 5 June, the higher water vapor mixing ratio observed at the exit areas, Beijung and Qingdao, showed some mixed zone from 2,000 to 3,000 m, and we interpreted this altitude as the local PBL height because it was developed by strong turbulent kinetic energy and entrainment with a simulated Ri_B of less than <5.0 up to around 2,000 m (not shown). The typical PBL structure was developed and expected to be maintained between 12 UTC on 5 June and 00 UTC on 6 June resulting in a sharply decreased water vapor mixing ratio up to the 2,000 m or higher in the PBL (i.e., Beijing and Qingdao), with no particular indication of tendencies to mix moistures uniformly in the vertical, which can be referred to as EML, from the above four sites of the exit area: Beijing, Qingdao, Sheyang, and Shanghai (Figure 7).

However, over the entrance area, the signature of the EML is found, clearly in Osan and Gwangju (Figure 7). The lower layer, at around an altitude of 1.5 (±0.5) km above the ground level, is isolated from both the free atmosphere (i.e., above the 3,000 m) and the lower atmosphere adjacent to the surface. We tried to find the EML by diagnosing with the lowest Ri_B above local PBL. Here EML top was diagnosed in qualitative manner as a level whose Ri_B starts to increase rapidly; thus, the layer is believed to act as a capping stable layer to trap the LRT pollutants within EML. In Figure 7, the simulated bulk Richardson numbers Ri_B are in the range of 1.2–6.1 within EML in the entrance area. This is indicating that atmospheric stability of EML is near neutral (or slightly stable) condition with the Ri_B of ~6 in the EML, where still the turbulence is expected to mix pollutants and moistures. However, the Ri_B in the upper atmosphere above EML showed higher values by factors of 2–5 or more over the same entrance area. The detailed vertical distributions of Ri_B were listed in Figure S2. Therefore, it was recognized that the EML was formed against the shallow MBL, making the upstream plumes be transported with little deposition/dissolution that occurs near ocean surface.

Figure 8 shows the simulated SO_2 and SO_4^{-2} concentrations at four sites located over the exit area at 12 UTC on 5 June, and at three sites over the entrance area at both 00 UTC and 06 UTC on 6 June. In Figure 8, EML's role in trapping air pollutants were also found. As in Figure 8, appreciable differences were shown between two areas. Over the exit area, there was no shifted or trapped air pollution with relatively higher concentrations on the surface, sharply decreasing with height up to the 4,000–3,000 m. In contrast, over the entrance area, pollution remains trapped within the boundary layer at around the 1,500 m at 00 UTC, strongly reflecting the existence of the EML at the entrance area near the KP. At 06 UTC, however, surface concentrations were relatively higher over the entrance area, showing that the trapped pattern existed at most sites and then gradually collapsed, at the Osan site in particular, due to local surface emissions.

Figure 9 shows airborne observations superposed on the simulated $PM_{2.5}$ over the YS for both two cases: LRT case (6 June 2015) and non-LRT case (2 June 2015). On 6 June 2015, both aircraft measurements and model results over the YS indicate that an elevated layer of high $PM_{2.5}$ concentration occurred at an altitude ≥1.2 km (Figure 9a), whereas there has been no particular evidence of EML over YS on 2 June 2015 (Figure 9b). As the airborne observations have a high spatiotemporal resolution, they can be scanned and the three-dimensional structures can be detected in detail, providing the vertical profiles of $PM_{2.5}$ concentrations over the YS. On 6 June 2015, although the model has a relatively lower spatiotemporal resolution, Figure 8 does exhibit an important vertical shape for the significant isolated plume when it appeared over the YS. This is also obvious in the Figure S4, which also shows the same patterns of concentrations of chemical components: SO_4^{-2}, NO_3^-, and NH_4^+, along the flight path across the Yellow Sea for both 6 and 2 June 2015. The high $PM_{2.5}$ and high ion concentration layer at an altitude of around 1 km or higher appeared at a similar location as the independent lower layer, just as the previously examined water vapor vertical distribution (Figures 9 and S4). The confirmation that the previously examined WRF-Chem model results matches well with meteorological measurements, and the distributions of aircraft measurements supports the idea that the EML exists, into which transported pollutants are trapped as they pass from high-emission regions to the upper marine atmosphere.

3.4. Transport and Transformation of Chinese Emissions

As previously explained, pollutants move along the EML to the downwind region during the LRT process. The air quality over the downwind region can be affected accordingly by the characteristics of the EML, and chemical transformation can be processed therein. To examine this role of the EML in chemical

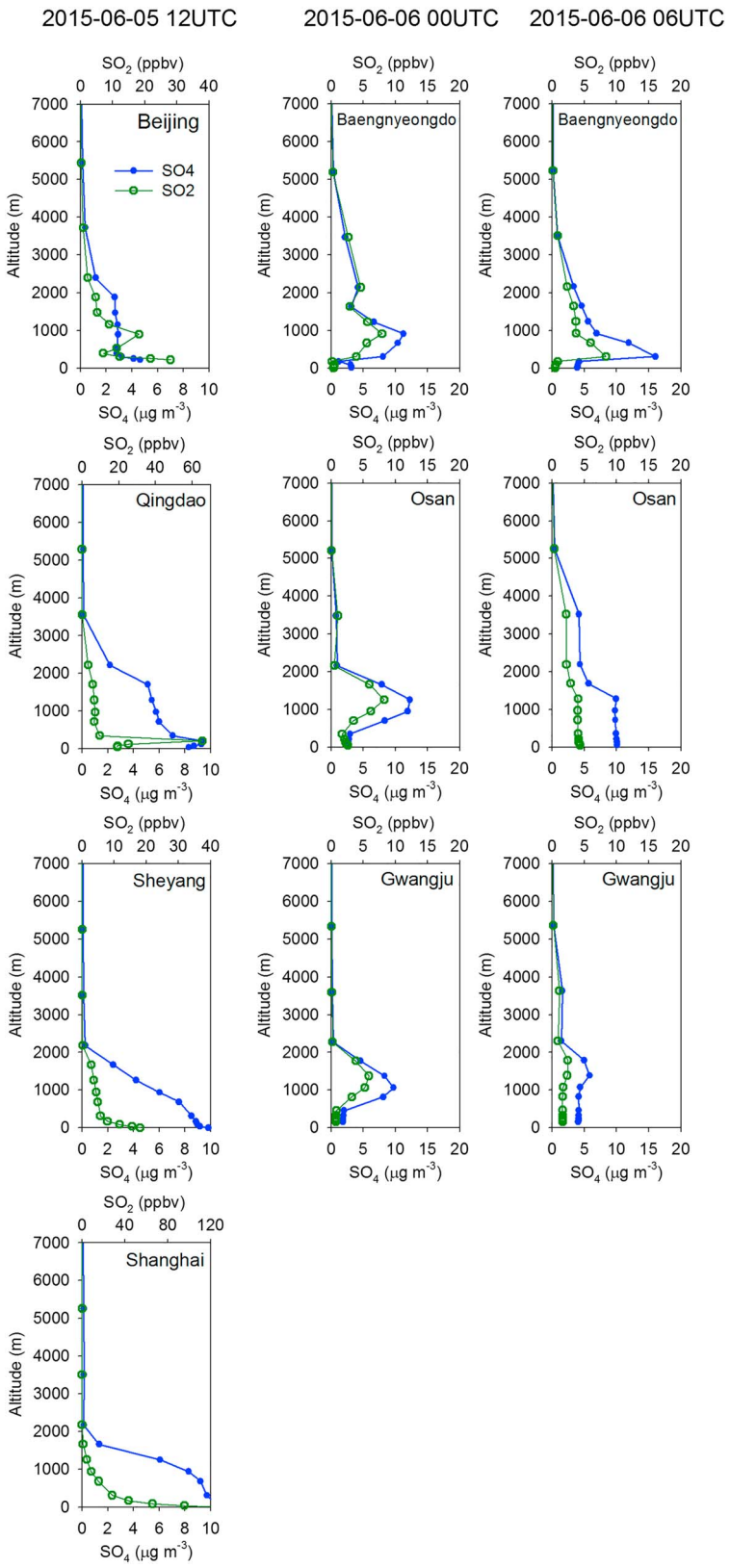


Figure 8. Vertical profiles of simulated SO_2 and SO_4^{-2} concentrations, for Beijing, Qingdao, Sheyang, and Shanghai at 12 UTC June 05 (left column), and for Baengnyeongdo, Osan, and Gwangju at 00 UTC (middle column) and 06 UTC (right column) on 6 June.

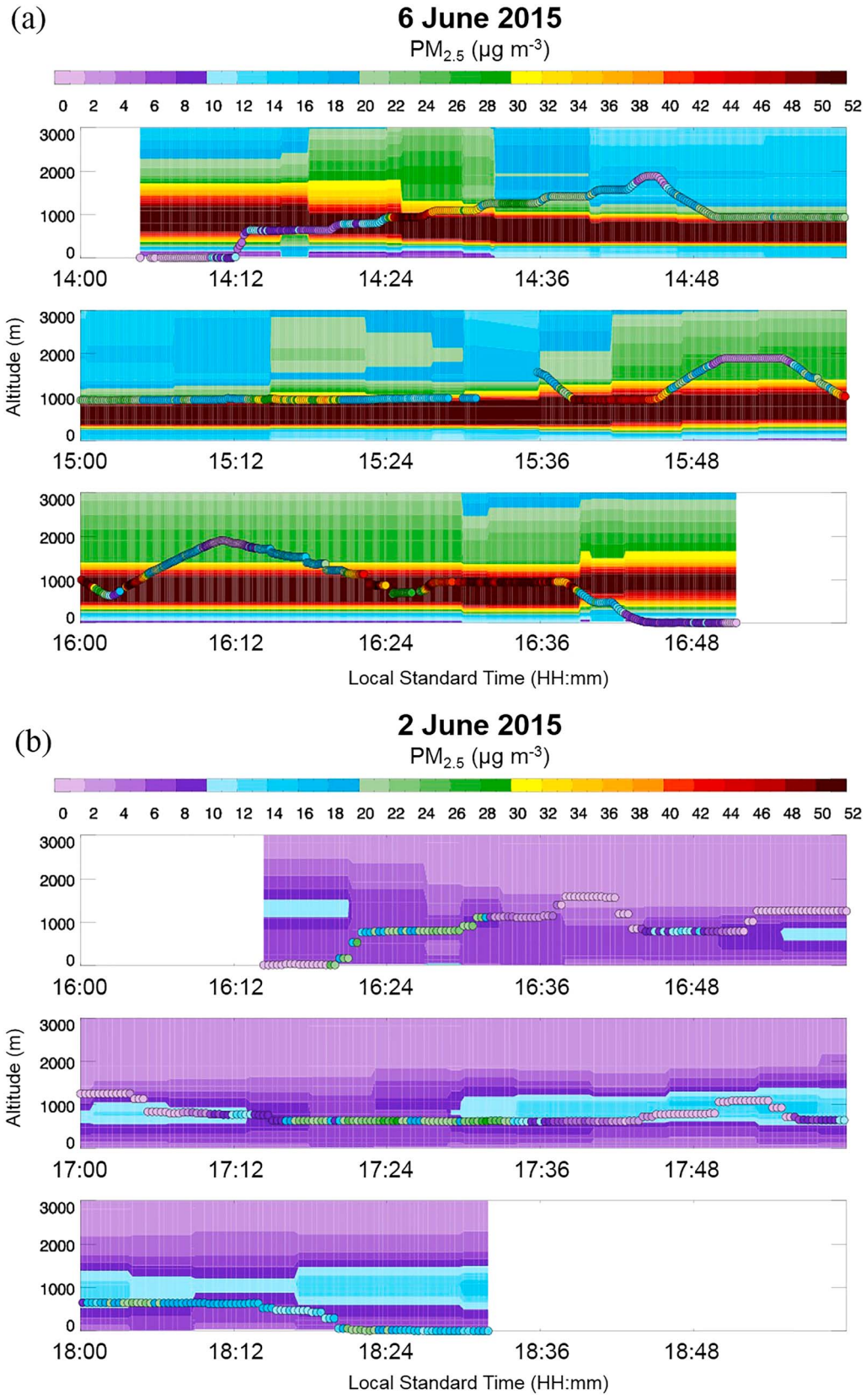


Figure 9. $PM_{2.5}$ concentrations along the flight path across the Yellow Sea on (a) 6 June and (b) 2 June 2015. The colored circles and shadings indicates airborne observations and model results, respectively.

process in detail, we examined the vertical distribution of the simulated chemical components of $PM_{2.5}$ within the EML above the YS at 03:00, 09:00, 15:00, and 21:00 LST on 6 June 2015.

Figure 10 shows the cross sections of $PM_{2.5}$ and simulated PBL heights (black dots) at 03:00, 09:00, 15:00, and 21:00 LST for both two cases: LRT case (6 June 2015) and non-LRT case (2 June 2015). The latitude-averaged area is indicated in Figure 1. It is also interesting to note that as Figure 9a demonstrates, high $PM_{2.5}$ concentrations flowed onto the top of the MBL at 03:00 LST on 6 June 2015, originating from the high-emission region of the exit area in China, moved to the YS, arriving at an altitude of around 1.0 (±0.5–) km in and around the entrance area on 6 June 2015, as indicated in Figure 10a. Consideration of the fact that the simulated MBL height was less than 500 m over the YS, as indicated in Figure 10a, leads to the conclusion that the simulated plume locations are not within the MBL, but rather much above the top of the MBL, corresponding well to the location of the EML described in section 3.3. Therefore, pollutants emitted from China gradually flowed into the confined EML and have the capability to move further without the ocean effects of the YS, arriving higher altitude above the west coast and the KP. Contrary to the long range transport process of $PM_{2.5}$ concentrations (Figure 10a), there has been no transboundary process of higher $PM_{2.5}$ concentrations on 2 June 2015, showing no transboundary process exceeding the longitude of 124°E (Figure 10b).

As the morning approached (i.e., at 09:00 LST in Figure 10a), the surface $PM_{2.5}$ concentrations in LRT case increased within the PBL over the exit area around 122–124° E due to anthropogenic air pollutants emitted from the metropolises and industrial areas. The plume, which had already entered the top of the MBL above the YS, continued moving eastward, with the $PM_{2.5}$ concentrations gradually increasing. As daytime progressed (i.e., 15:00 LST), $PM_{2.5}$ concentrations increased more in the PBL and moved over the YS, finally arriving at the downwind region with concentrations increasing further.

Here the plume within the EML was not diluted much until it came into contact with the developed PBL over the inland of the entrance area. It first moved on top of the PBL of the inland of entrance area, then gradually moved to the lower altitudes below the PBL top, exhibiting the similar process of fumigation that observed from the tall chimney stacks near the coastal-industrial area. Therefore, there are differences in the surface $PM_{2.5}$ concentrations over the inland entrance area, depending on whether or not there is PBL development up to the EML height. The vertical structure of the PBL against the MBL is a critical factor in predicting the surface concentration on the downwind side where the LRT process takes place.

As evening progressed (i.e., 21:00 LST), with the small and weak independent plume simulated over the exit area, the $PM_{2.5}$ concentrations within the PBL mostly decreased. It is interpreted that pollutants can move toward the downwind side along the EML, which is located above the MBL (Figure 10a). Over the entrance area, such as in the 126–128° E region, we observed a lowered PBL height as nighttime progressed, and thus, pollutants existing within the EML did not flow into the PBL over the KP in the simulations, passing only above the entrance area.

We also traced the temporal changes in the horizontal and vertical distributions of the pollutants, while the LRT progressed. The results showed that the surface air quality of the downwind sides can be influenced by the PBL heights over three areas: exit, marine, and entrance areas. The eastern China inland serves as an exit area (source region and upwind side), the YS as a marine area (part of the transport path), and the KP as an entrance area (receptor region and downwind side). Therefore, pollutants distributed at a low PBL altitude in the exit area were unable to move a long distance and were rapidly deposited or dissolved on the ocean surface. In contrast, pollutants mixed within the PBL at high altitudes could move along a layer that grew into the shape of the EML, and they were able to pass over the ocean area, moving down to the downwind region only at a time when the PBL of the entrance area developed up to high altitudes in the EML. Unless the PBL of the entrance area develops sufficiently, the LRT pollutants have little influence on the surface, only passing through the upper layer over the entrance area.

We also determined that there was a considerable increase in the simulated $PM_{2.5}$ concentrations within the MBL above the YS. This was due to an increase in aerosol formation processes as Chinese emissions of aerosol precursors moved through the YS region where water vapor is plentiful in the marine atmosphere, and the hygroscopic growth process of $PM_{2.5}$ can strongly impact the aerosol production. To identify the detailed hygroscopic growth over the YS, gas to particle conversions were examined using the WRF-Chem simulations for SO_2 and SO_4^{-2}.

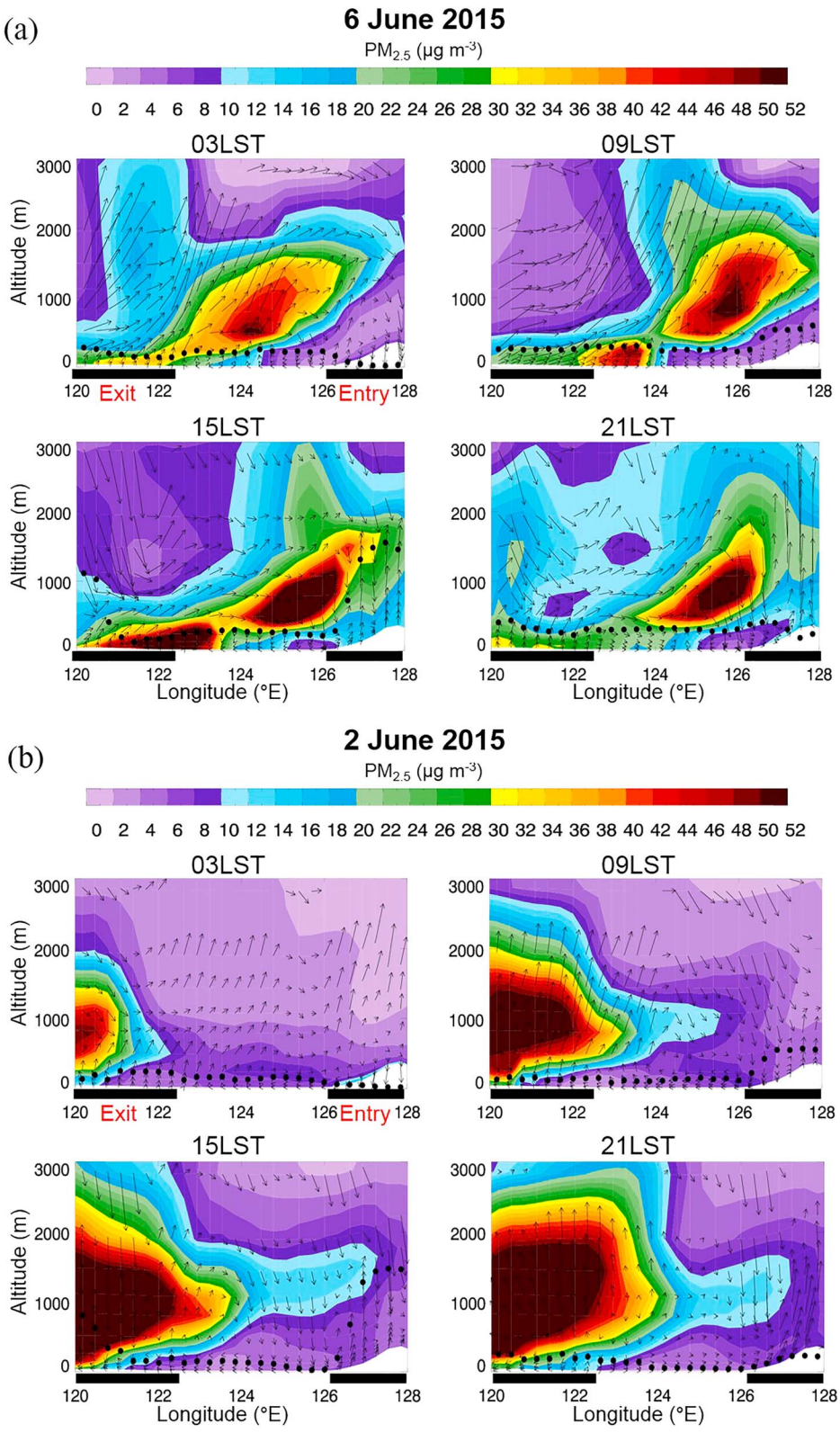


Figure 10. Curtain plots of Weather Research and Forecasting model coupled to Chemistry (WRF-Chem) simulated $PM_{2.5}$ concentrations averaged over areas ranging from 36° to 37°N at 03, 09, 15, 21 LST on (a) June and (b) 2 June 2015, respectively. The black dotted lines represent the planetary boundary layer height derived from WRF-Chem model simulations.

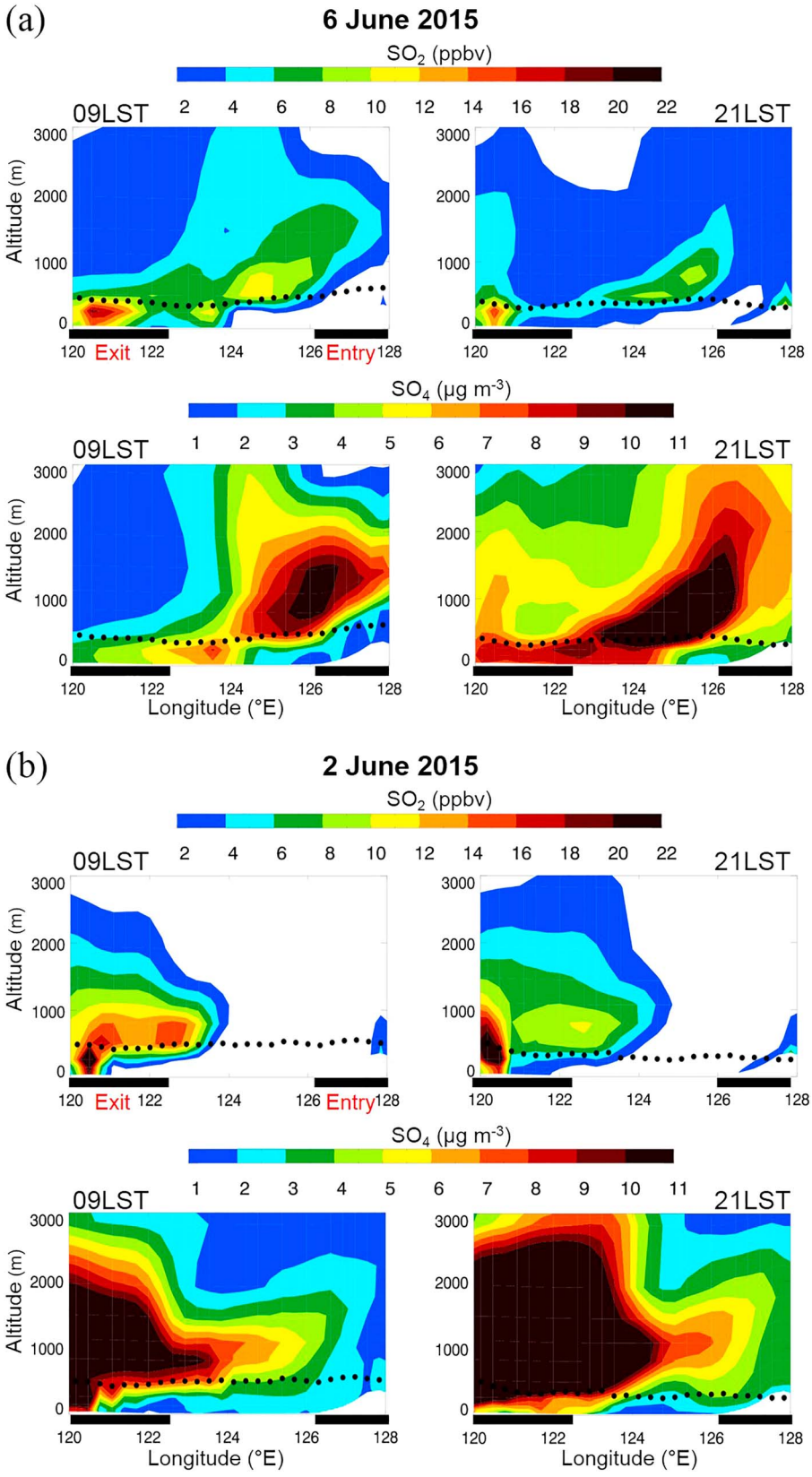


Figure 11. Vertical distributions of SO_2 and SO_4^{-2} concentrations averaged over areas ranging from 36°–37°N at 09 (left panels) and 21 local standard time (LST; right panels) on (a) 6 June 2015 and (b) 2 June 2015, respectively.

Figure 11 shows the vertical distribution of SO_2 and SO_4^{-2} concentration at 09:00 and 21:00 LST, respectively, on both cases: LRT case (6 June 2015) and non-LRT case (2 June 2015). As with the similar distributions, there was little transboundary process of higher SO_2 concentrations over YS on 2 June 2015 (Figure 11b). However, it is interesting to note that SO_4^{-2} concentrations increased at 21:00 LST up to around 3 km above the PBL but not transported across the longitude of 124°E (Figure 10b). On the contrary, on 6 June 2015, the SO_4^{-2} concentrations easily increased due to higher water vapor mixing ratios among the components of particulate matter (Figure 10a). The SO_2 concentration at 09:00 LST around the exit area covering the 120–122° E source areas was comparatively high, showing potential for partial movement into the PBL up to around 124°E but not flow to the YS (Figure 11a). In addition, we observed high SO_2 concentration in the EML above the MBL in the YS at 09:00 LST, while the SO_2 concentration within the EML had decreased at 21:00 LST on 6 June 2015. In the case of SO_4^{-2}, however, a high concentration plume appeared over the MBL at 09:00 LST, and the simulated SO_4^{-2} concentration within the PBL at the source region in China and the EML above the MBL both increased at 21:00 LST, on 6 June 2015 (Figure 11a).

The increase in both SO_2 and SO_4^{-2} concentrations in the emission source region can be affected by both chemical processes and diurnal variations in local emissions. However, in the case where the plume over the MBL had already moved to the YS, the changes in concentration were interpreted as a production via chemical transformation. Therefore, an examination of the PM concentrations for LRT case over the period from the nighttime on the previous day to the next morning revealed that the precursor SO_2 decreased while SO_4^{-2} increased as time passed. This tendency in both SO_2 and SO_4^{-2} concentrations was due to the aerosol nucleation process–SO_2 can be transformed to SO_4^{-2} as SO_2 passes within the EML, and SO_4^{-2} increases through the hygroscopic growth process in the marine atmosphere.

In the current study, we determined that the extent that pollutant transport from exit area can affect air quality over the entrance area is dependent on the vertical atmospheric structure in both areas, and their roles of PBL over both areas are of importance for the transport distance and mechanisms of inflow/outflow. This is an important controlling factor for transboundary issue. In addition, as pollutants are emitted from exit area and transported over the YS, a chemical transformation process occurs, transforming the pollutants from gaseous precursor matter to particulate matter within the EML in the marine atmosphere. This is another important controlling factor in air quality prediction in the area covering the Beijing-Shandong-YS-KP or Shanghai-YS-KP belt areas in northeast Asia.

4. Conclusions

In this study, we featured the meteorological and chemical mechanisms of LRT pollutants over northeast Asia during the MAPS-Seoul 2015 field campaign. We used a variety of observation data such as sonde observations, satellite image, and WRF-Chem modeling results and interpreted the detailed structure of the LRT mechanisms of Chinese plumes, which emit, transport, and impact on the concentrations of particulate matter in downwind regions. Our results indicate that in the prediction of the PM_{10} and $PM_{2.5}$ inflows by LRT process, the PBL conditions of the source area and conditions of receptor regions are both important for determining the extent of pollutant inflow from outside.

Sonde observations and WRF-Chem simulations show that when vertically well-mixed pollutants arrive at an altitude of 1–3 km in source emission regions, such as Chinese urban and industrial areas at daytime, their concentrations remain high within the EML above the nocturnal boundary layer at nighttime. In our study, EML observed in the marine atmosphere around the YS. The simulated bulk Richardson numbers (Ri_B) within EML were in the range of 1.2–6.1 in and around the western coast of the KP, showing the atmospheric stability of near-neutral or slightly stable conditions.

The observations indicate that the synoptic weather conditions relating to horizontal wind fields in the source and transport regions, and the PBL conditions in the receptor regions, can lead the LRT pollutants to reach the KP and affect its surface air quality. We concluded that pollutants can travel further via EML and, on the next day, it can influence the concentrations over the downstream region, implying that EML plays an important role in determining the air quality of capital area and west coast regions in Korea. However, when the PBL height in the China inland is low, Chinese emitted pollutant plumes passing

through the YS in the lower marine atmosphere are not able to travel further but are removed over the ocean surface, thereby having a small effect on the surface in Korea.

Notably, the model results show that as LRT pollutants pass over the YS, $PM_{2.5}$ concentrations can increase within the EML through hygroscopic process due to the plentiful water vapor in the marine atmosphere. These results show increases in concentrations of secondary aerosols within the EML, created by precursor matter, and enhancements in concentrations of the primary particulate matter. This secondary aerosol undergoes chemical transformation within the EML during the LRT process, which can further worsen the air quality in the KP located in the downwind region.

In addition, aircraft observations and model simulations showed other possible fates of LRT of $PM_{2.5}$ plume over the YS. The first is the lower PBL case over the source region, where $PM_{2.5}$ plume was trapped within the lower MBL during the LRT process. Second is a case for lower PBL in the receptor region, where LRT pollutants only pass through approximately 1.5 km height of downstream region. Therefore, in the future, we plan to use KORUS-AQ airborne observation data to examine the fates of air pollutants in more quantitative way. Together with those fates of air pollutants, we suggest considering the chemical transformation processes that can occur during the LRT process in the marine atmosphere where there are greater water vapor mixing ratios. In order to consider the complex chemical transformation processes, we plan to make an additional analysis on various chemical species measured during the KORUS-AQ campaign, including ozone and nitrate, during the LRT over northeast Asia.

Acknowledgments
The authors thank the National Institute of Environmental Research (NIER), South Korea, for providing surface air quality observations and aircraft measurement during MAPS-Seoul 2015 campaign period. All the data used are listed in the references or archived at http://www.airkorea.or.kr. This research was supported by Basic Science Research Program through the National Research Foundation of Korea (NRF) funded by the Ministry of Education (NRF-2015R1D1A1A01 060088 and NRF-2019R1I1A0A 01060445). The first and corresponding authors acknowledge support of Si-Wan Kim with installation of WRF-Chem model during the period of NOAA visiting scientist program.

References

Ackermann, I. J., Hass, H., Memmesheimer, M., Ebel, A., Binkowski, F. S., & Shankar, U. (1998). Modal aerosol dynamics model for Europe: Development and first applications. *Atmospheric Environment*, *32*(17), 2981–2999. https://doi.org/10.1016/S1352-2310(98)00006-5

Canagaratna, M. R., Jayne, J. T., Jimenez, J. L., Allan, J. D., Alfarra, M. R., Zhang, Q., et al. (2007). Chemical and microphysical characterization of ambient aerosols with the aerodyne aerosol mass spectrometer. *Mass Spectrometry Reviews*, *26*(2), 185–222. https://doi.org/10.1002/mas.20115

Carmichael, G. R., Calori, G., Hayami, H., Uno, I., Cho, S. Y., Engardt, M., et al. (2002). The MICS-Asia study: Model intercomparison of long-range transport and sulfur deposition in East Asia. *Atmospheric Environment*, *36*, 175–199.

Chen, F., & Dudhia, J. (2001). Coupling and advanced land surface-hydrology model with the Penn State-NCAR MM5 modeling system. Part I: Model implementation and sensitivity. *Monthly Weather Review*, *129*, 569–585.

Choi, J.-K., Heo, J.-B., Ban, S. -J., Yi, S.-M., & Zho, K.-D. (2013). Source appointment of $PM_{2.5}$ at the coastal area in Korea. *Science of the Total Environment*, *447*, 370–380. https://doi.org/10.1016/j.scitotenv.2012.12.047

Chun, Y., Boo, K.-O., Kim, J., Park, S.-U., & Lee, M. (2001). Synopsis, transport, and physical characteristics of Asian dust in Korea. *Journal of Geophysical Research*, *106*(D16), 18,461–18,469. https://doi.org/10.1029/2001JD900184

DeCarlo, P. F., Kimmel, J. R., Trimborn, A., Northway, M. J., Jayne, J. T., Aiken, A. C., et al. (2006). Field-deployable, high-resolution, time-of-flight aerosol mass spectrometer. *Analytical Chemistry*, *78*(24), 8281–8289. https://doi.org/10.1021/ac061249n

Dickerson, R. R., Li, C., Li, Z., Marufu, L. T., Stehr, J. W., McClure, B., et al. (2007). Aircraft observations of dust and pollutants over northeast China: Insight into the meteorological mechanisms of transport. *Journal of Geophysical Research*, *112*, D24S90. https://doi.org/10.1029/2007JD008999

Drewnick, F., Hings, S. S., DeCarlo, P., Jayne, J. T., Gonin, M., Fuhrer, K., et al. (2005). A new time-of-flight aerosol mass spectrometer (TOF-AMS): Instrument description and first field deployment. *Aerosol Science and Technology*, *39*(7), 637–658. https://doi.org/10.1080/02786820500182040

Emmons, L. K., Walters, S., Hess, P. G., Lamarque, J.-F., Pfister, G. G., Fillmore, D., et al. (2010). Description and evaluation of the model for ozone and related chemical Tracers, version 4 (MOZART-4). *Geoscientific Model Development*, *3*(1), 43–67. https://doi.org/10.5194/gmd-3-43-2010

Grell, G. A., & Freitas, S. (2014). A scale and aerosol aware stochastic convective parameterization for weather and air quality modeling. *Atmospheric Chemistry and Physics*, *14*(10), 5233–5250. https://doi.org/10.5194/acp-14-5233-2014

Grell, G. A., Peckham, S. E., McKeen, S., Schmitz, R., Frost, G., Skamarock, W. C., & Eder, B. (2005). Fully coupled "online" chemistry within the WRF model. *Atmospheric Environment*, *39*(37), 6957–6975. https://doi.org/10.1016/j.atmosenv.2005.04.027

Guenther, A., Karl, T., Harley, P., Wiedinmyer, C., Palmer, P. I., & Geron, C. (2006). Estimates of global terrestrial isoprene emissions using MEGAN (Model of Emissions of Gases and Aerosols from Nature). *Atmospheric Chemistry and Physics*, *6*(11), 3181–3210. https://doi.org/10.5194/acp-6-3181-2006

Holzer, M., Hall, T. M., & Stull, R. B. (2005). Seasonality and weather-driven variability of transpacific transport. *Journal of Geophysical Research*, *110*, D23103. https://doi.org/10.1029/2005JD006261

Iacono, M. J., Delamere, J. S., Mlawer, E. J., Shephard, M. W., Clough, S. A., & Collins, W. D. (2008). Radiative forcing by long-lived greenhouse gases: Calculations with the AER radiative transfer models. *Journal of Geophysical Research*, *113*, D13103. https://doi.org/10.1029/2008JD009944

Janjic, Z (2002), Nonsingular implementation of the Mellor–Yamada level 2.5 scheme in the NCEP meso model. NCEP Office Note No. 437, 60.

Jayne, J. T., Leard, D. C., Zhang, X. F., Davidovits, P., Smith, K. A., Kolb, C. E., & Worsnop, D. R. (2000). Development of an aerosol mass spectrometer for size and composition analysis of submicron particles. *Aerosol Science and Technology*, *33*(1-2), 49–70. https://doi.org/10.1080/027868200410840

Jeong, U., Lee, H., Kim, J., Kim, W., Hong, H., & Song, C. K. (2013). Determination of the inter-annual and spatial characteristics of the contribution of long-range transport to SO_2 levels in Seoul between 2001 and 2010 based on conditional potential source contribution function (CPSCF). *Atmospheric Environment*, *70*, 307–317. https://doi.org/10.1016/j.atmosenv.2013.01.009

Jimenez, J. L. (2003). Ambient aerosol sampling using the AerodyneAerosol Mass Spectrometer. *Journal of Geophysical Research*, *108*(D7), 8425. https://doi.org/10.1029/2001JD001213

Jo, H. Y., & Kim, C. H. (2013). Identification of long-range transported haze phenomena and their meteorological features over Northeast Asia. *Journal of Applied Meteorology and Climatology*, *52*(6), 1318–1328. https://doi.org/10.1175/JAMC-D-11-0235.1

Kim, C.-H., Lee, H.-J., Kang, J.-E., Jo, H.-Y., Park, S.-Y., Jo, Y.-J., et al. (2018). Meteorological overview and signatures of long-range transport processes during the MAPS-Seoul 2015 campaign. *Aerosol and Air Quality Research*, *18*(9), 2173–2184. https://doi.org/10.4209/aaqr.2017.10.0398

Kim, H. C., Kim, E., Bae, C., Cho, J. H., Kim, B. U., & Kim, S. (2017). Regional contributions to particulate matter concentration in the Seoul Metropolitan Area, Korea: Seasonal variation and sensitivity to meteorology and emission inventory. *Atmospheric Chemistry and Physics*, *17*(17), 10,315–10,332. https://doi.org/10.5194/acp-17-10315-2017

Kim, J., Choi, D., Koo, Y., Lee, J., & Park, H. (2016). Analysis of domestic and foreign contributions using DDM in CMAQ during articulate matter episode period of February 2014 in Seoul. *Journal of Korean Society for Atmospheric Environment*, *32*(1), 82–99. https://doi.org/10.5572/KOSAE.2016.32.1.082

Kim, S.-W., Heckel, A., Frost, G. J., Richter, A., Gleason, J., Burrows, J. P., et al. (2009). NO_2 columns in the western United States observed from space and simulated by a regional chemistry model and their implications for NO_x emissions. *Journal of Geophysical Research*, *114*, D11301. https://doi.org/10.1029/2008JD011343

Kim, S.-W., Yoon, S.-C., & Kim, J. (2008). Columnar Asian dust particle properties observed by sun/sky radiometers from 2000 to 2006 in Korea. *Atmospheric Environment*, *42*(3), 492–504. https://doi.org/10.1016/j.atmosenv.2007.09.055

Kumar, R., Naja, M., Pfister, G. G., Barth, M. C., Wiedinmyer, C., & Brasseur, G. P. (2012). Simulations over South Asia using the weather research and forecasting model with chemistry (WRF-Chem): Chemistry evaluation and initial results. *Geoscientific Model Development*, *5*(3), 619–648. https://doi.org/10.5194/gmd-5-619-2012

Kwon, H.-J., Cho, S.-H., Chun, Y., Lagarde, F., & Pershagen, G. (2002). Effects of the Asian dust events on daily mortality in Seoul, Korea. *Environmental Research*, *90*(1), 1–5. https://doi.org/10.1006/enrs.2002.4377

Lamsal, L. N., Martin, R. V., van Donkelaar, A., Celarier, E. A., Bucsela, E. J., Boersma, K. F., et al. (2010). Indirect validation of tropospheric nitrogen dioxide retrieved from the OMI satellite instrument: Insight into the seasonal variation of nitrogen oxides at northern midlatitudes. *Journal of Geophysical Research*, *115*, D05302. https://doi.org/10.1029/2009JD013351

Lee, S. J., Kim, J., & Cho, C. H. (2014). An automated monitoring of atmospheric mixing height from routine radiosonde profiles over South Korea using a web-based data transfer method. *Environmental Monitoring and Assessment*, *186*(5), 3253–3263. https://doi.org/10.1007/s10661-014-3615-y

Lee, T., Choi, J., Lee, G., Ahn, J., Park, J. S., Atwood, S. A., et al. (2015). Characterization of aerosol composition, concentrations, and sources at Baengnyeong Island, Korea using an aerosol mass spectrometer. *Atmospheric Environment*, *120*, 297–306. https://doi.org/10.1016/j.atmosenv.2015.08.038

Levelt, P. F., van den Oord, G. H. J., Dobber, M. R., Mälkki, A., Visser, H., de Vries, J., et al. (2006). The Ozone Monitoring Instrument. *IEEE Geoscience and Remote Sensing*, *44*(5), 1093–1101. https://doi.org/10.1109/TGRS.2006.872333

Li, C., Krotkov, N. A., Dickerson, R. R., Li, Z., Yang, K., & Chin, M. (2010). Transport and evolution of a pollution plume from northern China: A satellite-based case study. *Journal of Geophysical Research*, *115*, D00K03. https://doi.org/10.1029/2009JD012245

Li, C., Stehr, J. W., Marufu, L. T., Li, Z. Q., & Dickerson, R. R. (2012). Aircraft measurements of SO_2 and aerosols over northeastern China: Vertical profiles and the influence of weather on air quality. *Atmospheric Environment*, *62*, 492–501. https://doi.org/10.1016/j.atmosenv.2012.07.076

Li, Z., Chen, H., Cribb, M., Dickerson, R., Holben, B., Li, C., et al. (2007). Preface to special section on East Asian Studies of Tropospheric Aerosols: An International Regional Experiment (EASTAIRE). *Journal of Geophysical Research*, *112*, D22S00. https://doi.org/10.1029/2007JD008853

Liang, Q., Jaeglé, L., Jaffe, D. A., Weiss-Penzias, P., Heckman, A., & Snow, J. A. (2004). Long-range transport of Asian pollution to the northeast Pacific: Seasonal variations and transport pathways of carbon monoxide. *Journal of Geophysical Research*, *109*, D23S07. https://doi.org/10.1029/2003JD004402

Lin, C., Liu, S., Chou, C., Huang, S., Liu, C., Kuo, C., & Young, C. (2005). Long-range transport of aerosols and their impact on the air quality of Taiwan. *Atmospheric Environment*, *39*(33), 6066–6076. https://doi.org/10.1016/j.atmosenv.2005.06.046

Lin, M., Fiore, A. M., Horowitz, L. W., Cooper, O. R., Naik, V., Holloway, J., et al. (2012). Transport of Asian ozone pollution into surface air over the western United States in spring. *Journal of Geophysical Research*, *117*, D00V07. https://doi.org/10.1029/2011JD016961

Liu, H., Jacob, D. J., Bey, I., Yantosca, R. M., Duncan, B. N., & Sachse, G. W. (2003). Transport pathways for Asian pollution outflow over the Pacific: Interannual and seasonal variations. *Journal of Geophysical Research*, *108*(D20), 8786. https://doi.org/10.1029/2002JD003102

Miao, Y., Guo, J., Liu, S., Zhao, C., Li, X., Zhang, G., et al. (2018). Impacts of synoptic condition and planetary boundary layer structure on the trans-boundary aerosol transport from Beijing-Tianjin-Hebei region to northeast China. *Atmospheric Environment*, *181*, 1–11. https://doi.org/10.1016/j.atmosenv.2018.03.005

NCEP (2000), NCEP FNL Operational model global tropospheric analyses, continuing from July 1999. Research Data Archive at the National Center for Atmospheric Research, Computational and Information Systems Laboratory, Boulder, CO, https://doi.org/10.5065/D6M043C6

Orlando, J. J., Tyndall, G. S., Bertman, S. B., Chen, W., & Burkholder, J. B. (2002). Rate coefficient for the reaction of OH with MPAN. *Atmospheric Environment*, *36*(11), 1895–1900. https://doi.org/10.1016/S1352-2310(02)00090-0

Park, I.-S., Choi, W.-J., Lee, T.-Y., Lee, S.-J., Han, J.-S., & Kim, C.-H. (2005). Simulation of long-range transport of air pollutants over Northeast Asia using a comprehensive acid deposition model. *Atmospheric Environment*, *39*(22), 4075–4085. https://doi.org/10.1016/j.atmosenv.2005.03.038

Sander, S. P., Golden, D. M., Kurylo, M. J., Moortgat, G. K., Wine, P. H., Ravishankara, A. R., et al. (2006). Chemical kinetics and photochemical data for use in atmospheric studies evaluation number 15, Publication 06-2, Jet Propulsion Laboratory, Pasadena, CA.

Schell, B., Ackermann, I. J., Hass, H., Binkowski, F. S., & Ebel, A. (2001). Modeling the formation of secondary organic aerosol within a comprehensive air quality model system. *Journal of Geophysical Research*, *106*(D22), 28,275–28,293. https://doi.org/10.1029/2001JD000384

Skamarock, W. C., Klemp, J. B., Dudhia, J., Gill, D. O., Barker, D. M., Duda, M. G., et al. (2008). *A description of the advanced research WRF version 3, Techni-cal Note 475 + STR*. Boulder, CO, USA: National Center for Atmospheric Research.

Stockwell, W. R., Kirchner, F., Kuhn, M., & Seefeld, S. (1997). A newmechanism for regional atmospheric chemistry modeling. *Journal of Geophysical Research*, *102*, 15,847–25,879.

Sun, W.-Y., Yang, K. J.-S., & Lin, N.-H. (2013). Numerical simulations of Asian dust-aerosols and regional impact on weather and climate, Part II: PRCM-dust model simulation. *Aerosol and Air Quality Research*, *13*(6), 1641–1654. https://doi.org/10.4209/aaqr.2013.06.0208

Tyndall, G. S., Cox, R. A., Granier, C., Lesclaux, R., Moortgat, G. K., Pilling, M. J., et al. (2001). Atmospheric chemistry of small organic peroxy radicals. *Journal of Geophysical Research*, *106*(D11), 12,157–12,182. https://doi.org/10.1029/2000JD900746

Uno, I., Eguchi, K., Yuminoto, K., Takemura, T., Shimizu, A., Uematsu, M., et al. (2009). Asian dust transported one full circuit around the globe. *Nature Geoscience*, *2*(8), 557–560. https://doi.org/10.1038/ngeo583

Woo, J.-H., Quan, S., Choi, K.-C., Kim, H., Jin, H., Song, C.-K., et al. (2014), Development of the Comprehensive Regional Emissions Inventory for Atmospheric Transport Experiment (CREATE) inventory in support of integrated modeling of climate and air quality for east Asia. In: 16th GEIA Conference. NCAR, Boulder, CO, USA.

Zhang, L., Jacob, D. J., Boersma, K. F., Jaffe, D. A., Olson, J. R., Bowman, K. W., et al. (2008). Transpacific transport of ozone pollution and the effect of recent Asian emission increases on air quality in North America: An integrated analysis using satellite, aircraft, ozonesonde, and surface observations. *Atmospheric Chemistry and Physics*, *8*(20), 6117–6136. https://doi.org/10.5194/acp-8-6117-2008